Breakdown of temporal-coupled-mode theory under multiple excitations with destructive interference

L. Simonson,[1,2] S. Ozdemir,[3] K. Busch,[4,5] and R. El-Ganainy[1,2,*]

[1]*Department of Physics, Michigan Technological University, Houghton, Michigan 49931, USA*

[2]*Henes Center for Quantum Phenomena, Michigan Technological University, Houghton, Michigan 49931, USA*

[3]*Department of Engineering Science and Mechanics, and Materials Research Institute, The Pennsylvania State University, University Park, Pennsylvania 16802, USA*

[4]*Humboldt-Universität zu Berlin, Institut für Physik, AG Theoretische Optik and Photonik, D-12489 Berlin, Germany*

[5]*Max-Born-Institut, D-12489 Berlin, Germany*

(Received 27 February 2024; accepted 24 July 2024; published 5 September 2024)

Temporal-coupled-mode theory (TCMT) is an important tool that is widely used for analyzing and designing integrated photonic systems that consist of multiple connected resonators. In microresonator systems with well-separated modes (relatively large free spectral range compared to the modal width), standard TCMT accounts only for the resonant excitation and is known to give excellent results in the weak-coupling limit. In this paper, we reveal a peculiar situation where TCMT breaks down under multiple excitation conditions. As we demonstrate, this can be explained by the destructive and the constructive interference of the excitations associated to the resonant and off-resonant modes respectively. In this case, we show that a multimode TCMT should be employed to account for these effects. Our results thus suggest that, while it is safe to use the standard TCMT under a single excitation, it must be applied with care when multiple excitations are involved.

DOI: 10.1103/PhysRevA.110.033509

I. INTRODUCTION

The unprecedented progress in integrated photonics over the past two decades has been largely enabled by the development of various electromagnetic design toolboxes. Typically, these involve separately computing the response of a few elements via (numerically exact) Maxwell solvers (e.g., via finite element [1], finite difference time domain [2], or Fourier modal methods [3]) and extracting from them waveguide dispersion relations, resonator frequencies and linewidths, mode profiles, (complex) reflection and transmission coefficients, coupling coefficients, etc. These results are then fed into (approximate) circuit-modeling methods for the efficient analysis of more complex systems such as the scattering matrix approach [4] and different flavors of coupled-mode theory (CMT) [5–8]. Conversely, device designs based on the scattering matrix technique or from CMT approaches are typically validated via Maxwell solvers.

Among the different flavors of CMT, temporal-coupled-mode theory (TCMT) [5,9] has become a relevant tool for understanding and engineering photonic integrated circuits based on coupled microresonators in the weak-coupling regime. The scattering matrix approach can be used to study the same problem, yet it requires more careful and lengthy calculations in order to ensure the consistency of boundary conditions along closed light trajectories. On the other hand, TCMT reduces the problem to rather small sets of coupled ordinary differential equations. In linear systems, these take the form of a discrete Schrodinger equation, where the physics of the problem is encoded in a finite system matrix, which is often denoted as H. In turn, this provides a useful tool for engineering photonic structures such as slotted ring resonators [10], nonreciprocal devices [11], and systems with non-Hermitian symmetries [12–14] or topological invariance [15,16]. Moreover, TCMT can be enriched by including material nonlinearities and dispersion to derive the Lugiato-Lefever equation [17] that accounts for various phenomena such as frequency comb generation, soliton crystals, and wave mixing inside microring resonators [18]. In quantum optics, the quantum Langevin equation [19] plays the role of TCMT after promoting the c variables to bosonic creation and annihilation operators and adding the appropriate noise terms that ensure the conservation of the bosonic commutation relation.

Given the success of TCMT and its widespread use in applications ranging from non-Hermitian and topological photonics to nonlinear and quantum optics and also given the fact that current photonic systems are becoming increasingly more complex with many integrated components on the same chip, it is reasonable to seek a complete understanding of the validity of TCMT and its potential failure. To date, it was assumed that TCMT can be always applied in the weak-coupling regime where one assumes that the coupling between the various optical elements does not significantly alter their bare eigenmodes. In this paper, however, we uncover a peculiar situation where the application of TCMT may give very erroneous results under multiple excitation conditions, even when the system operates in the weak-coupling regime. This is particularly important because some optical functionalities, such as coherent perfect absorption [20–23] and tailoring the

*Contact author: ganainy@mtu.edu

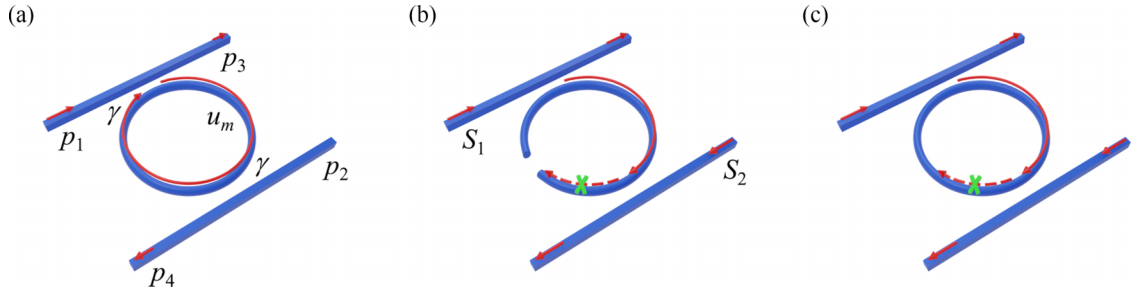

FIG. 1. A schematic demonstrating the main effect studied in this paper. (a) An optical system made of a microring resonator evanescently coupled to two waveguides serving as input and output channels. Under a single excitation from port p_1 with a frequency matching the real part of the resonance frequency associated with the CW mode u_m, only this mode is predominantly populated. (b) If a section of the microring is removed, the resonator becomes a curved waveguide. In this case, spatial coupled mode analysis can be used to analyze the system. Within this framework, it is possible to tailor a second excitation from port p_2 such that the net outcome is a destructive interference in the curved waveguide section marked by the dashed arrow and the "X" sign, indicating the absence of light. Clearly, adding back that section does not alter the light distribution. Thus, even for the full system, it is possible to judicially chose the amplitudes and phases of the two excitations to produce a nonuniform light distribution inside the microring resonator as schematically shown in (c).

response of photonic chips [24–27], can be achieved only by using multiple excitations.

II. RESULTS

A. Concept

Let us consider a microring resonator symmetrically coupled to two waveguides as shown in Fig. 1(a). In the absence of any excitation, one can solve Maxwell's equations under outgoing boundary conditions to find the resonant modes of the ring, which are also known as the quasinormal modes (QNMs) [28,29] and their associated complex eigenfrequencies. When light is excited from one port [say, port p_1 in Fig. 1(a)], some of these modes become populated with different weights that depend on the excitation frequency and modal overlap. Thus, in general the field inside the resonator can be expressed as $E(\mathbf{r},t)=\sum_n u_n(t)\mathcal{E}_n(\mathbf{r})$, where $\mathcal{E}_n(\mathbf{r})$ is the field distribution of the QNM characterized by the index n as a function of the spatial coordinates $\mathbf{r}$ and $u_n(t)$ is a time dependent amplitude. When the excitation frequency is close to one of the resonance frequencies, say that corresponding to mode m, the above expansion can be approximated by the resonant term whose amplitude, $u_m(t)$, evolves according to the TCMT. This is the situation depicted schematically in Fig. 1(a), where the excitation from port p_1 populates the clockwise (CW) traveling mode inside the ring resonator. Note that in the absence of the waveguides, the QNMs of the microring resonator are rotationally symmetric. While the presence of the waveguides breaks this rotational symmetry, in the weak-coupling regime, this effect is very weak. In this case, the light intensity inside the microring resonator will be almost uniform across its perimeter.

The above picture is generally assumed to apply when two or more excitations are involved. To understand that, let us consider the situation where another input from port p_2 is also used (i.e., both are exciting the CW mode); the standard TCMT reads (we neglect intrinsic losses)

$$\frac{du_m}{dt}=(i\omega_m-2\gamma)u_m+\sqrt{2\gamma}(\tilde{S}_1+e^{-i\theta_m^{(1)}}\tilde{S}_2), \qquad (1)$$

where ω_m is the resonance frequency, γ is the loss rate due to the coupling to each waveguide, and the excitations from the two waveguides are given by $\tilde{S}_1$ and $\tilde{S}_2$. Importantly, $\theta_m^{(1)}$ represents the phase acquired by the CW wave as it travels from the junction with waveguide 1 to that with waveguide 2. Here, $\theta_m^{(1)}$ depends on the relative locations of the two waveguides and the propagation constant β_m of the waveguide mode inside the ring waveguide. Note that $\tilde{S}_{1,2}$ are not field amplitudes. Rather, $|\tilde{S}_{1,2}|^2$ is proportional to the electromagnetic power in each waveguide, respectively. Under continuous wave excitation at resonance, i.e., when $\tilde{S}_{1,2}=S_{1,2}e^{i\omega_m t}$, the steady-state field amplitude inside the ring is given by $U_m=\frac{1}{\sqrt{2\gamma}}(S_1+e^{-i\theta_m^{(1)}}S_2)$, where $u_m(t)=U_m e^{i\omega_m t}$. Thus, it is clear that regardless of the values and phases of $S_{1,2}$ and the phase $\theta_m^{(1)}$, TCMT predicts that the light intensity inside the ring will just follow the distribution of the quasinormal mode $\mathcal{E}(\mathbf{r})$ [up to a factor $u(t)$]. Given that the external signals both couple to the CW mode, which is a traveling wave, it follows that TCMT predicts a uniform distribution of the light intensity (not necessarily the field) across the perimeter of the ring. In order to appreciate the problem with this conclusion, let us now consider the situation depicted in Fig. 1(b) where a section of the ring resonator is removed altogether, effectively turning it into a curved waveguide. This system can now be described by using spatial coupled mode theory that describes light tunneling between waveguides. For the same double excitations from ports p_1 and p_2, one can easily tune the input intensities and phases (i.e., the complex quantities S_1 and S_2) in order to have a destructive interference in the curved waveguide section marked by the dashed arrow and the green "X" sign which indicate that light does not couple to that section of the curved waveguide. In other words, under this condition, the field amplitude at the output section of the central waveguide (the region marked by the "X" sign) is zero and thus all the input light from ports p_1 and p_2 exits from ports p_3 and p_4. Obviously, in that case, the field and intensity distribution of light inside the curved waveguide will be highly nonuniform (there is light in the right section of the curved waveguide marked by the continuous red arrow but not in the left section marked by the "X" sign and dashed red

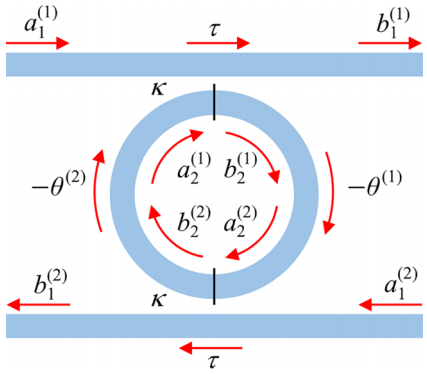

FIG. 2. An identical microring resonator system to that shown in Fig. 1(a) with parameters and fields labels suitable for scattering matrix analysis. The coupling junctions depicted here (the black bars at the top and bottom of the ring) are assumed to be zero width. $\theta^{(1,2)}$ are the acquired phases for the right and left halves of the ring, respectively. Note that for a resonant mode $\theta^{(1,2)} \equiv \theta_m^{(1,2)}$, whereas for any off-resonant mode with an index n the subindex m is replaced by n.

arrow). The crucial observation here is that adding back the removed section while at the same time keeping all the input values intact [Fig. 1(c)] will not have any impact on the field distribution because the field amplitude at this added section is zero. It is thus clear that the predictions of the TCMT cannot give the correct results in this last scenario.

To confirm the above predictions, we now employ the scattering matrix approach to analyze the problem shown in Fig. 2 in detail and determine the values of the input power signals and their relatives phases that tune the system to this peculiar operating point. In this case, the input and output field amplitudes, which we denote as $a_1^{(1,2)}$ and $b_1^{(1,2)}$, together with the field amplitudes inside the ring just before and after the junction, which are denoted by $a_2^{(1,2)}$ and $b_2^{(1,2)}$, are connected by the relation

$$\begin{pmatrix} b_1^{(1,2)} \\ b_2^{(1,2)} \end{pmatrix} = \begin{pmatrix} \tau & i\kappa \\ i\kappa & \tau \end{pmatrix} \begin{pmatrix} a_1^{(1,2)} \\ a_2^{(1,2)} \end{pmatrix}, \tag{2}$$

where τ and κ are the real-valued transmission and coupling coefficients as shown in Fig. 2 and they satisfy the power conservation relation $\tau^2 + \kappa^2 = 1$. In writing the above relation, we assumed that the junction has vanishing length. Of course, in reality, the field tunnels between the waveguide and the resonator across a finite length. However, this simplification does not affect the main conclusion of our paper as will soon be seen from the corresponding full-wave simulations. In addition to the above scattering formula, we also have the following relation: $a_2^{(1,2)} = b_2^{(2,1)} e^{-i\theta^{(2,1)}}$, implying that $|a_2^{(1,2)}|^2 = |b_2^{(2,1)}|^2$, i.e., constant power at either side of each junction. In what follows, we will assume the waveguides are located symmetrically on each side of the resonator and hence $\theta_m^{(1)} = \theta_m^{(2)} = \theta_m$. The mode quantization condition is thus given by $2\theta_m \equiv \beta_m L = 2m\pi$ for any integer m where β_m is the propagation constant associated with the microring waveguide mode and L is the total length of the microring perimeter. In practice, this relation is meaningful only for larger m values (typically larger than 20) in order to have modes with high quality factors. By using the above relations, we find that $b_2^{(1,2)} = \frac{i}{\kappa}(a_1^{(1,2)} + \tau a_1^{(2,1)} e^{-im\pi})$ (see Appendix A for details). Accordingly,

$$\eta \equiv \frac{|E_{\text{right}}|}{|E_{\text{left}}|} = \frac{|b_2^{(1)}|}{|b_2^{(2)}|} = \frac{|a_1^{(1)} + \tau a_1^{(2)} e^{-im\pi}|}{|a_1^{(2)} + \tau a_1^{(1)} e^{-im\pi}|}. \tag{3}$$

Here, E_{right} and E_{left} are the complex-valued components of the electric field perpendicular to the plane of the ring located at the midpoints of the right and left halves of the ring, respectively [see the red "X"s in Fig. 3(a)]. Obviously, the value of η is not necessarily close to unity as otherwise predicted by TCMT. In fact, the input fields can be chosen to result in the extreme situation of the field being zero on one side of the ring, i.e., $\eta = 0$ or ∞. For instance, the latter choice, which corresponds to $|E_{\text{left}}| = 0$, can be achieved when $a_1^{(2)} = \mp\tau a_1^{(1)}$ with the minus or plus signs chosen for m even or odd, respectively. Importantly, we emphasize that the above result is valid even in the weak-coupling regime, i.e., when $\kappa \ll 1$, which confirms our initial intuition that, under certain multiexcitation conditions, the TCMT can fail even in this regime.

B. Full-wave simulations

Next, we verify these results by performing a full-wave analysis using the COMSOL software package, which is based on the finite element method suitable for irregular geometries. Here, the structure under consideration is shown in Fig. 3(a) together with the corresponding dimensions and material parameters which are chosen to be relevant to that of silicon photonics platforms.

Importantly, to ensure we are in the weak-coupling regime, we chose a relatively large gap between the waveguides and the ring resonators, namely $d = 300$ nm. For this design, we find that $\tau^2 = 0.9865$ and $\kappa^2 = 0.0135$ which confirms operation in the weak-coupling limit. The quality factor of this device is $Q = 15200$ (see Appendix B). This relatively large value of Q is chosen to illustrate that our results are valid in the weak-coupling regime. In Appendix C, we present more results for the case of a stronger coupling. In our simulations and without loss of generality, we focus on the quasinormal mode with $m = 57$. Full-wave modal analysis shows that the real part of the complex resonance frequency of that mode is $f_0 = 193.5579$ THz. In order to target that mode, we launch waves in the waveguides with that resonance frequency (later we will scan the input frequency to determine the optimal operating point that maximizes the mode asymmetry parameter η). As a reference point, we first present the simulation results under a single excitation, i.e., $a_1^{(1)} = 1$ and $a_1^{(2)} = 0$ (using arbitrary units since the system is linear) as shown in Fig. 3(b). Clearly, the field along the ring is uniform with $\eta \approx 1.01$ which confirms operation in the weak-coupling regime as described before. Here, $\eta \equiv \frac{|E_{\text{right}}|}{|E_{\text{left}}|}$ where the fields are measured at the red "X" points along the ring in Fig. 3(a).

Next, we test the extreme asymmetric field distribution scenario discussed above by using two excitations with $a_1^{(1)} = 1$ and $a_1^{(2)} = \tau$. Note that, since in our case $m = 57$, we have $e^{-i\theta_m} = -1$. As a result, at each junction, the fields inside the ring interfere destructively. The difference in their amplitudes

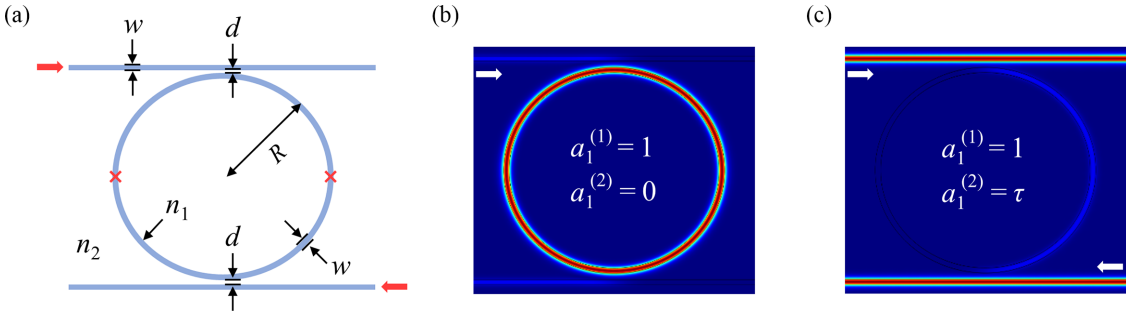

FIG. 3. (a) A schematic diagram of the actual photonic structure used in the full-wave simulations with the following geometric and material parameters: $R = 5$ μm (outer radius), $w = 250$ nm, $d = 300$ nm (edge-edge separation), the waveguide refractive index $n_1 = 3.48$, while the background index $n_2 = 1.45$. The red "X"s denote the points where field values are measured. (b) The magnitude of the complex-valued electric-field distributions inside the structure at resonance under a single excitation of amplitude $a_1^{(1)} = 1$ shown by the white arrow (top left waveguide port). Here, one can observe that the field distribution is almost uniform. (c) Same as in (b) after adding a second resonant excitation of magnitude $a_1^{(2)} = \tau$ from the right port of the lower waveguide. In this case, the field asymmetry between the left and right sides of the microring resonator is clear, which indicates the breakdown of the standard TCMT analysis. In these simulations, the coupling between the waveguides and the ring was chosen to be very weak to emphasize that the effect is not due to strong coupling. In Appendix C, we consider more commonly used coupling conditions.

is chosen to produce a zero field in the left side of the ring (see the scattering matrix analysis in the previous section). However, due to the finite junction size and the adiabatic coupling between the waveguide and the ring, the field does not completely vanish everywhere. Instead, as shown in Fig. 3(c), a clear and strong asymmetry in the field distribution with $\eta \approx 285$ can be observed. Another important observation is that the total energy inside the ring in Fig. 3(b) is much larger than the case in Fig. 3(c) (the ratio is $\approx 10^4$), which is also consistent with the scattering matrix analysis outlined above. This point will be discussed further on.

To check the feasibility of observing such an effect in practice, we perform a sensitivity analysis and plot the field asymmetry ratio, η, as a function of the excitation frequency, phase difference between excitation waves ($\delta\theta_m$), and the deviation from the optimal amplitude ratio. The results are depicted in Fig. 4. From these plots, we can conclude that the effect is resilient against frequency change (large values of η can still be obtained for δf in the range of MHz). The amplitudes and phases require stronger but realistic control. As a side note, we observe that the maximum asymmetry is not achieved at the exact resonance frequency but rather is shifted by -40 MHz and also occurs for $\delta\theta_m = -4$ mrad. This can probably be explained by the fact that our prediction for these values based on the scattering matrix approach does not account for the finite length of the resonator-waveguide junction.

C. Field expansion in terms of the eigenmodes

While the above analysis and computational results clearly demonstrate the potential failure of TCMT under certain input conditions, they do not provide an insight into the reason behind this effect in terms of the QNMs of the resonator. In principle, this can be done by projecting the asymmetric field on the QNMs. This however can be a cumbersome process since the QNMs are in general not orthogonal [28,29] and one needs to solve an adjoint problem and use biorthogonality [28,30,31]. In microring resonators supporting high-quality modes, the QNMs are tightly confined inside the ring, so we can focus only on the azimuthal dependence of the mode, simplifying the analysis (as the modes are nearly orthogonal), and also provide a deeper understanding of the results. Specifically, we can approximate the QNMs by $|E_n(r,\phi)\rangle = |R(r)\rangle\,|\Phi_n(\phi)\rangle$. In writing the above expression, we assumed

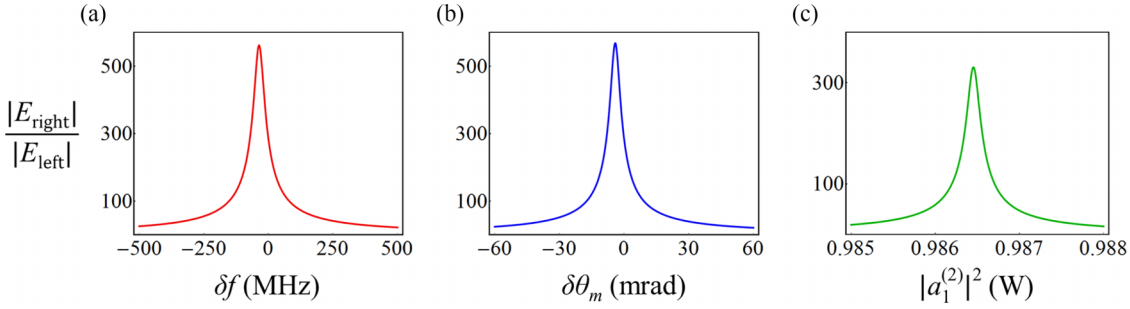

FIG. 4. Plots of the asymmetry parameter $\frac{|E_{\text{right}}|}{|E_{\text{left}}|}$ as functions of δf (a), $\delta\theta_m$ (b), and $|a_1^{(2)}|^2$ (c). Clearly, the field asymmetry can be still observed for a range of input parameters. As discussed in the text, the maximum asymmetry occurs for an input frequency and phase that is shifted from the ideal conditions derived from the scattering matrix analysis. A possible explanation is that in our analysis, we considered a zero size coupling junction between each waveguide and the ring resonator.

that the field distribution of the QNM can be approximately factorized into two separate functions of the coordinates r and ϕ, where the radial part r does not depend on the quantization index n. This approximation is reasonable for two reasons: the ring is made of a single-mode waveguide with a radius almost ten times larger than the wavelength, λ, inside the ring, and the free spectral range (FSR) is a small fraction of the wavelength (FSR $\approx \lambda/57$ for our ring parameters). Hence, the radial parts of wave functions associated with the neighboring modes are almost identical and resemble the transverse mode distribution of the straight waveguide. Furthermore, we will use the normalizations $\langle R|R\rangle = 1$ and $\langle \Phi_n|\Phi_n\rangle = 1$. Here we assume the electric field to be polarized in the z direction, i.e., perpendicular to the ring plane, and hence one can employ the standard complex scalar inner product used in quantum mechanics. In this regime, it is easy to see that $|\Phi_n(\phi)\rangle = \frac{1}{\sqrt{2\pi}} e^{-in\phi}$. Note that $\langle \Phi_n|\Phi_m\rangle = \delta_{n,m}$. By recalling that under the extreme asymmetry condition the scattering matrix method predicts the presence of the field only in the right side of the ring and vanishing field in the left side, we can then express the field distribution as $|E(r,\phi)\rangle = |R(r)\rangle\,|\Phi(\phi)\rangle$, where $|\Phi_m(\phi)\rangle = i\kappa e^{-im\phi}$ for $0 < \phi < \pi$ and $|\Phi(\phi)\rangle = 0$ for $\pi < \phi < 2\pi$, where m is the quantization number associated with the resonant mode under consideration (recall that in our simulations $m = 57$). Here, we took the point of the junction 1 as the reference point for $\phi = 0$ and assumed that ϕ rotates CW. By using the expansion $E(r,\phi) = \sum_n c_n E_n(r,\phi)$, and the above relations, we find $c_n = \frac{\kappa}{\sqrt{2\pi}(n-m)}[e^{i(n-m)\pi} - 1]$ (see Appendix D for a detailed calculation). In other words, $c_m = i\kappa\sqrt{\pi/2}$, $c_n = -\sqrt{\frac{2}{\pi}}\frac{\kappa}{(n-m)}$ when $(n-m)$ is an odd number, and $c_n = 0$ otherwise. Note that the above expression predicts that c_n is finite for certain values of $n < 0$. This is counterintuitive since it means that there is energy transfer from the waveguides to the counterclockwise (CCW) modes. We believe this to be an artifact originating from our assumption of zero junction length and hence a uniform field across the right side of the ring. In reality, the waveguides approach the ring adiabatically and the field will vary across the perimeter which will eventually lead to vanishing CCW fields in the absence of any other source of back reflection. The important point to emphasize here is that the Fourier series components for the QNMs having quantization numbers n in the vicinity of the resonant mode m are comparable to the coefficient associated with mode m itself (for instance, $|c_{57}/c_{56}| = \pi/2$). It is this interference between these modes that results in the sharp asymmetry in the field distribution.

To better understand why these modes are excited with comparable efficiency, we plot a schematic diagram for the optical response associated with the QNMs as shown in Fig. 5. This response function could be for example the transmission in an add-drop filter configuration. Due to the finite quality factor of every mode, the response is a Lorentzian curve rather than a delta function. Under a single excitation at resonance with mode m, only that mode is highly excited. Note that the neighboring modes are also excited but with a much lower efficiency as depicted in the figure using the blue and green arrows. On the other hand, under a double excitation, each mode is driven by a term of the form $S_1 + e^{-i\beta_n L/2} S_2$, where L is the length of the microring, i.e., its perimeter. Here $\beta_n \equiv \beta_n(\omega)$ is the propagation constant associated with the ring waveguide mode of QNM n. Even when the waveguide is single moded, the fact that each QNM has a different resonance frequency means that β_n varies from one mode to another. For the resonant mode with $n = m$, we have $e^{-i\beta_m L/2} \approx -1$ for odd values of m (which is the situation considered in our full-wave simulation example), weakly exciting the resonant mode and bringing its excitation amplitude to those associated with the neighboring QNMs having even values of n with $e^{-i\beta_n L/2} \approx 1$. This picture provides a direct insight into the formation of the asymmetric field distribution described above. In addition, it also provides a powerful predictive tool to tailor this behavior in photonic systems. For instance, based on this analysis, one would expect this effect to be more pronounced in larger resonators with smaller free spectral range. On the other hand, it predicts that this effect cannot be observed in single-mode resonators such as those implemented using photonic crystal structures [32,33] unless radiation modes are invoked.

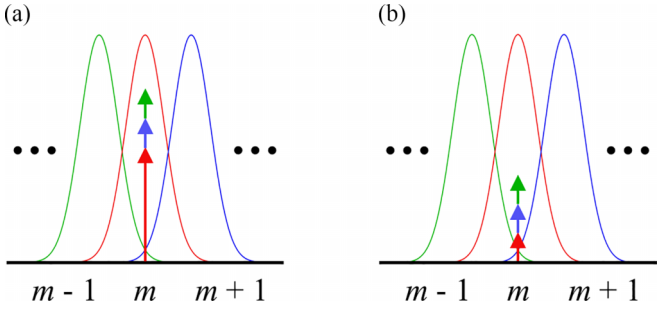

FIG. 5. A schematic of the response function (an add-drop configuration for example) associated with the resonant mode m and the neighboring modes $m \pm 1$. Due to the modal losses, the response function has a finite linewidth. The overlap between the tails of the modes is exaggerated for illustration only. In the presence of an input signal, different modes can be excited depending on their spatial and spectral overlap with the input signal. Under a single excitation that exhibits significant spatial overlap and resonance frequency matching with mode m, only that mode will be dominantly excited with much smaller excitations of the neighboring modes (assuming, of course, that there is an overlap between the excitation signal and all of the relevant modes). This situation is depicted in (a) where the strength of the excitation is schematically represented by the arrows (note that the contribution from modes $m \pm 1$ is exaggerated here for illustration). When two different excitations are used and their amplitudes and phases are adjusted to significantly reduce the overlap between the collective excitation and the resonant mode m, it is possible for the modes m, $m \pm 1$ (as well as other neighboring modes) to have comparable amplitudes as shown schematically by the length of arrows in (b). In that case, the interference between these modes can lead to a nonuniform field distribution along the microring resonator.

D. Multimode TCMT

The discussion above suggests that TCMT can still be used to obtain the correct results if one considers coupling to many QNMs instead of just the resonant mode. To illustrate this point, let us consider again the case where the resonant state corresponds to an odd value of m. In that case, the steady-state field amplitude of that mode is [see

Eq. (1) and its solution] $U_m = \frac{1}{\sqrt{2\gamma}}(S_1 - S_2)$ (recall that in that case, $\theta_m^{(1)} \equiv \beta_m L/2$ is an odd multiple of π and hence $e^{-i\theta_m^{(1)}} = -1$). Conversely, for an off-resonant mode with an even n (for which $e^{-i\theta_n^{(1)}} = 1$), the field amplitude is given by $U_n = \frac{\sqrt{2\gamma}}{i(\omega_n - \omega_m) + 2\gamma}(S_1 + S_2)$. Qualitatively, it is clear from the above expression that if $S_1 \sim S_2$, both U_m and U_n can be comparable in magnitude despite the fact that U_m is excited at resonance. But, we can make this discussion even more quantitative by noting that in the weak-coupling regime, $\gamma \ll$ FSR. Thus, we can write $U_n \approx \frac{\sqrt{2\gamma}}{i(\omega_n - \omega_m)}(S_1 + S_2)$. By using $\omega_n = \beta_n v_p = 2\pi n v_p/L$, where v_p is the phase velocity, we finally obtain $U_n = \frac{i\sqrt{2\gamma}L}{2\pi(n-m)v_p}(S_1 + S_2)$. Furthermore, since τ is very close to unity, it follows that $S_1 + S_2 \approx 2S_1$ (recall that in this paper we consider the excitation $S_2 \sim \tau S_1$) and hence $U_n \approx \frac{i\sqrt{2\gamma}L}{\pi(n-m)v_p}S_1$. Next, we evaluate the resonant term U_m. The excitation term in this case is given by $S_1 - \tau S_1 = S_1 - \sqrt{1-\kappa^2}S_1 \approx \frac{\kappa^2}{2}S_1$. We note then that from the scattering matrix analysis, the relative energy lost from the resonator to the waveguides is $\kappa^2 + \tau^2\kappa^2 \approx 2\kappa^2$. Since the time it takes for a round trip is $T = L/v_p$, we find the energy loss rate to be $\frac{2\kappa^2 v_p}{L}$. Finally, from TCMT, we know that the energy loss rate in the resonator is 4γ. Putting these results together, we obtain that $\frac{\kappa^2 v_p}{2\gamma L} \approx 1$. It follows that the multimode TCMT gives identical results to the Fourier coefficients obtained from the transmission matrix method, namely $U_n/U_m = c_n/c_m$. Thus, it is clear that the correct physical behavior can be retrieved by using a multimode TCMT that accounts for the off-resonant excitations of multiple longitudinal modes.

Before we conclude, we make the following important remarks. First, in demonstrating the breakdown of the standard TCMT associated with the field asymmetry under multiple excitations, we have used a lossless microring resonator. If the ring has intrinsic losses, the field amplitude will decay along the propagation direction. In that case, the main result of this paper is still valid but for different relative amplitudes and phases of the two input signals (different values are needed to produce the destructive interference on one side of the ring). Second, in addition to the very different output power distribution under single and double excitations [see Figs. 3(b) and 3(c)], our results are also relevant to the situation where a third waveguide is coupled to the ring at the location of the "X" sign on the left side of the ring in Fig. 3(a) or in the case where plasmonic particles or nanoantennas are deposited on the ring (see for example [34]) at the aforementioned position. In either of these situations, the light coupled out of the ring will strongly depend on the excitation condition.

III. CONCLUSION

In summary, we have demonstrated that standard TCMT can fail even in the weak-coupling regime where it is assumed to always hold. Our analysis based on the scattering matrix method of microring resonators, which is also confirmed by using full-wave simulations of Maxwell's equations, clearly shows that under certain multiexcitation conditions, the energy distribution inside the ring is highly nonuniform with the light more concentrated in one-half of the ring. This is in stark contrast to TCMT which predicts uniform light distribution. To better understand this behavior, we have expressed the steady-state, nonuniform field distribution inside the resonator in terms of its QNMs. In doing so, we have taken advantage of the relatively high Q factor of the resonator and assumed that the QNMs are orthogonal, which is a condition that will clearly not apply in resonators with low Q factors. Finally, we have shown that one can still retrieve the correct results from TCMT by accounting for not only the resonant mode excitation but the off-resonant modes as well. Given the wide range of applications where TCMT is typically employed for performing a fast analysis, our results indicate that the application of TCMT must be considered with caution.

ACKNOWLEDGMENTS

This work is supported by the AFOSR Multidisciplinary University Research Initiative Award on Programmable Systems with Non-Hermitian Quantum Dynamics (Grant No. FA9550-21-1-0202). R.E. also acknowledges support from NSF Grant No. ECCS 1807552 and the Alexander von Humboldt Foundation. L.S. acknowledges support from the SMART Scholarship.

APPENDIX A: FIELD AMPLITUDE CALCULATION

Here, we derive the expression that appears before Eq. (3) for the field amplitudes $b_2^{(1,2)}$ in terms of the input fields $a_1^{(1,2)}$ from ports p_1 and p_2, respectively. From the second line of Eq. (2), we have $b_2^{(1,2)} = i\kappa a_1^{(1,2)} + \tau a_2^{(1,2)}$. By noting that $a_2^{(1,2)} = b_2^{(2,1)} e^{-i\theta_m^{(2,1)}}$ and again using the second line of Eq. (2), we obtain $b_2^{(1,2)} = i\kappa a_1^{(1,2)} + \tau(i\kappa a_1^{(2,1)} + \tau b_2^{(1,2)} e^{-i\theta_m^{(1,2)}})e^{-i\theta_m^{(2,1)}}$. Finally, by using $\tau^2 + \kappa^2 = 1$ and $\theta_m^{(1)} = \theta_m^{(2)} = m\pi$, we obtain $b_2^{(1,2)} = \frac{i}{\kappa}(a_1^{(1,2)} + \tau a_1^{(2,1)} e^{-im\pi})$.

APPENDIX B: QUALITY FACTOR CALCULATION

The quality factor of the loaded resonator shown in Fig. 2 is given by $Q \equiv \omega_0/4\gamma$. Here, $\omega_0 = 1216.16$ THz, which corresponds to the $m = 57$ mode. The decay rate parameter γ can be obtained by considering the add-drop configuration and calculating the transmission from port p_1 to p_4 of Fig. 1(a). By following this standard procedure (see [35] for details), we estimate that $\gamma = 20$ GHz, and hence $Q = 15\,200$. We note that this relatively high Q value was chosen to emphasize that our results are valid even in the very weak-coupling regime.

APPENDIX C: NUMERICAL EXAMPLE FOR A STRUCTURE WITH A STRONGER COUPLING

In the main text, we demonstrated the breakdown of the TCMT for a system that exhibits very weak coupling between the microring resonator and the waveguide. Here, for completeness, we also present the full-wave simulation results for a more practical example where the separation between the ring and the waveguide is $d = 200$ nm, resulting in $\tau^2 = 0.9018$ and $\kappa^2 = 0.0979$, yielding a quality factor of $Q = 2134$. As can be seen in Figs. 6(a) and 6(b), our results persist: the TCMT works well for a single excitation and

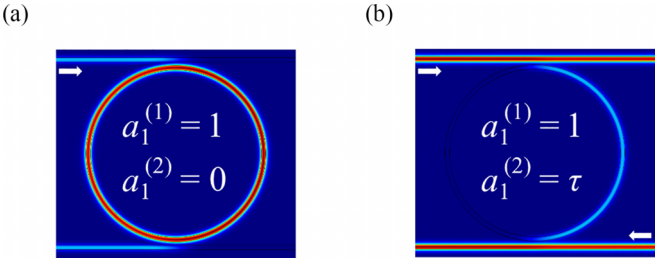

FIG. 6. (a) The magnitude of the complex-valued electric-field distributions inside the structure at resonance under a stronger-coupling condition (with $Q = 2134$) for a single excitation with amplitude $a_1^{(1)} = 1$ as shown by the white arrow (top left waveguide port) and (b) for a double excitation with $a_1^{(1)} = 1$ and $a_1^{(2)} = \tau$. Obviously, the same behavior observed in Figs. 3(b) and 3(c) persists here.

breaks down for a carefully selected double excitation (the amplitude and phase relation between the two excitations in this case are exactly the same for the structure used in the main text). In this last scenario, we found that $\eta \approx 418$.

APPENDIX D: FIELD EXPANSION CALCULATION

Within the context of the scattering matrix method, we have found that under a particular excitation (see the main text), light will exist only in half of the ring and will vanish in the other half, i.e., we provided an expansion of the asymmetric electric field in terms of the QNMs of the ring resonator: $|\Phi_m(\phi)\rangle = i\kappa e^{-im\phi}$ for $0 < \phi < \pi$ and $|\Phi(\phi)\rangle = 0$ for $\pi < \phi < 2\pi$. By choosing $\langle R|R\rangle = 1$ and $|\Phi_n(\phi)\rangle = \frac{1}{\sqrt{2\pi}} e^{-in\phi}$ to ensure that $\langle \Phi_n|\Phi_n\rangle = 1$, we evaluate the Fourier coefficients defined by $c_n = \frac{\langle E_n|E_m\rangle}{|E_n|^2}$ to be

$$c_n = \frac{i\kappa}{\sqrt{2\pi}} \int_0^{\pi} e^{in\phi} e^{-im\phi}\, d\phi = \frac{\kappa}{\sqrt{2\pi}(n-m)} [e^{i(n-m)\pi} - 1]. \tag{D1}$$

In deriving the above expression, we made the reasonable assumption that $|R\rangle$ is independent of the quantization indices and that the modes are quasiorthogonal, which is valid for resonators with relatively high quality factors.

[1] Ö. Özgün and M. Kuzuoğlu, *MATLAB-Based Finite Element Programming in Electromagnetic Modeling* (CRC, Boca Raton, FL, 2018).

[2] A. Z. Elsherbeni and V. Demir, *The Finite-Difference Time-Domain Method for Electromagnetics with MATLAB Simulations* (Scitech, Edison, NJ, 2015).

[3] H. Kim, J. Park, and B. Lee, *Fourier Modal Method and its Applications in Computational Nanophotonics* (CRC, Boca Raton, FL, 2017).

[4] B. E. A. Saleh and M. C. Teich, *Fundamentals of Photonics* (Wiley, New York, 2019).

[5] H. A. Haus, *Waves and Fields in Optoelectronics* (Prentice-Hall, Englewood Cliffs, NJ, 1984).

[6] J. Heebner, R. Grover, and T. Ibrahim, *Optical Microresonators: Theory, Fabrication, and Applications* (Springer, New York, 2007).

[7] V. Van, *Optical Microring Resonators: Theory, Techniques and Applications* (CRC, Boca Raton, FL, 2017).

[8] K. Okamoto, *Fundamentals of Optical Waveguides* (Academic, New York, 2021).

[9] W. Suh, Z. Wang, and S. Fan, IEEE J. Quant. Electron. **40**, 1511 (2004).

[10] K. R. Hiremath, J. Niegemann, and K. Busch, Opt. Express **19**, 8641 (2011).

[11] K. X. Wang, Opt. Lett. **43**, 5623 (2018).

[12] R. El-Ganainy, K. G. Makris, M. Khajavikhan, Z. H. Musslimani, S. Rotter, and D. N. Christodoulides, Nat. Phys. **14**, 11 (2018).

[13] L. Feng, R. El-Ganainy, and L. Ge, Nat. Photon. **11**, 752 (2017).

[14] Ş. K. Özdemir, S. Rotter, F. Nori, and L. Yang, Nat. Mater. **18**, 783 (2019).

[15] L. Lu, J. D. Joannopoulos, and M. Soljačić, Nat. Photon. **8**, 821 (2014).

[16] T. Ozawa, H. M. Price, A. Amo, N. Goldman, M. Hafezi, L. Lu, M. C. Rechtsman, D. Schuster, J. Simon, O. Zilberberg, and I. Carusotto, Rev. Mod. Phys. **91**, 015006 (2019).

[17] L. A. Lugiato, F. Prati, M. L. Gorodetsky, and T. J. Kippenberg, Phil. Trans. R. Soc. A **376**, 20180113 (2018).

[18] D. V. Strekalov, C. Marquardt, A. B. Matsko, H. G. L. Schwefel, and G. Leuchs, J. Opt. **18**, 123002 (2016).

[19] M. O. Scully and M. S. Zubairy, *Quantum Optics* (Cambridge University, Cambridge, England, 2012).

[20] Y. D. Chong, L. Ge, H. Cao, and A. D. Stone, Phys. Rev. Lett. **105**, 053901 (2010).

[21] D. G. Baranov, A. Krasnok, T. Shegai, A. Alù, and Y. Chong, Nat. Rev. Mater. **2**, 17064 (2017).

[22] R. R. Grote, J. B. Driscoll, and R. M. Osgood, Opt. Lett. **38**, 3001 (2013).

[23] Y. Slobodkin, G. Weinberg, H. Hörner, K. Pichler, S. Rotter, and O. Katz, Science **377**, 995 (2022).

[24] R. A. Cohen, O. Amrani, and S. Ruschin, Nat. Photon. **12**, 706 (2018).

[25] O. Daulay, G. Liu, K. Ye, R. Botter, Y. Klaver, Q. Tan, H. Yu, M. Hoekman, E. Klein, C. Roeloffzen, Y. Liu, and D. Marpaung, Nat. Commun. **13**, 7798 (2022).

[26] M. Kang, Z. Zhang, T. Wu, X. Zhang, Q. Xu, A. Krasnok, J. Han, and A. Alù, Nat. Commun. **13**, 4536 (2022).

[27] X. Jiang, S. Yin, H. Li, J. Quan, H. Goh, M. Cotrufo, J. Kullig, J. Wiersig, and A. Alù, Nat. Phys. **20**, 109 (2024).

[28] P. T. Kristensen, K. Herrmann, F. Intravaia, and K. Busch, Adv. Opt. Photon. **12**, 612 (2020).

[29] C. Gigli, T. Wu, G. Marino, A. Borne, G. Leo, and P. Lalanne, ACS Photon. **7**, 1197 (2020).

[30] N. Moiseyev, *Non-Hermitian Quantum Mechanics* (Cambridge University, Cambridge, England, 2011).

[31] T. Wu, D. Arrivault, W. Yan, and P. Lalannea, Comput. Phys. Commun. **284**, 108627 (2023).

[32] J. D. Joannopoulos, S. G. Johnson, J. N. Winn, and R. D. Meade, *Photonic Crystals: Molding the Flow of Light* (Princeton University, Princeton, NJ, 2008).

[33] K. Vahala, *Optical Microcavities* (World Scientific, Singapore, 2004).

[34] K. G. Cognée, H. M. Doeleman, P. Lalanne, and A. F. Koenderink, Light Sci. Appl. **8**, 115 (2019).

[35] Q. Zhong, A. Hashemi, Ş. K. Özdemir, and R. El-Ganainy, Phys. Rev. Res. **3**, 013220 (2021).